Model, Analysis and Application of Tubular Linear Switched Reluctance Actuator for Linear Compressors

***Abstract*— The tubular linear switched reluctance actuator (TLSRA) is presented in this paper, to propel linear compressors with oscillatory motion. The proposed TLSRA possess the advantages of higher force density and shorter magnetic flux paths in comparison with conventional LSRAs, and are much suitable for applications to reciprocating oscillation due to absence of any coils and magnets on mover in comparison with linear actuators with moveable permanent magnets. The analytical expression of gap permeance is proposed for fast machine design and optimization. The designed thrust force characteristics are verified by FEA and the experiment. The dynamic model of the linear compressor propelled by the proposed TLSRA is presented. The simulated and experimental results demonstrate that the developed TLSRA can be applied to linear oscillatory motion and that the developed linear compressor propelled by the proposed TLSRA is effective and feasible.**

***Index Terms*— Linear actuators, linear compressors, oscillatory motion, switched reluctance drives.**

I. Introduction

LINEAR reciprocating motion is required in some applications, such as pumps and compressors in refrigeration. As known well, a piston in conventional reciprocating pumps or compressors is usually driven by a rotary motor via a crank. This linear motion mechanism from rotary motor to crank-shaft results in more mechanical loss. Consequently, the system efficiency of linear compressors is low. The reciprocating piston is able to be directly driven by a linear actuator coupled with the resonant spring. The direct-drive solutions to the problem of the cylinder-wall wearing caused by the crank side force in conventional reciprocating compressors were reported and the whole system efficiency can be considerably improved. In previous studies, linear permanent magnet actuators are used to directly to drive linear compressors [1]-[8]. In [1], the numerical techniques to calculate coil inductance and magnet/coil coupling for arbitrary turn placement are presented for the design of air-core tubular linear electric drives, in which a permanent magnet (PM) moves relative to an air-core coil. The transverse-flux moving-magnet linear oscillatory actuator for a compressor is proposed in [2]. The reference [3] presents a new hybrid model and a testing sequence to characterize a small PM oscillatory motor for compressor-like applications, in which the radially magnetized tubular-shaped PM is on the axially moving parts. The overview of linear electric actuator and generator topologies, applications performance and design methodologies are presented in [4], including linear induction actuators, linear synchronous PM actuators, DC brush linear actuators, moving coil PM linear actuators, Sawyer linear motors, linear solenoid actuators, and linear-oscillatory actuators. In [5], the single-phase, tubular moving-magnet motor with homopolar radially magnetized magnets and stationary back-iron is proposed for applications of linear compressors. The reference [6] presents the computation of the thrust forces for permanent magnet transverse flux linear oscillating actuators with moving magnet. In [7], the permanent-magnet linear actuator for static and reciprocating short-stroke electromechanical systems is proposed, in which PMs are on the stator. However, the efficiency is low due to absence of a laminated magnetic circuit and the structure of the actuator is complicated. The moving-magnetic linear actuator is also proposed in [8]. A common feature of typical linear PM actuators discussed in those studies is that permanent magnets on movers/translators have to be moveable. Thus, those actuators result in complicated construction and high cost due to moveable permanent magnets, potential unreliability and possibly reduced lifetime due to frequently reciprocating shock to the mover/translator with permanent magnets. In this paper, the tubular linear switched reluctance actuator (TLSRA) is proposed to directly drive pumps or compressors. Without any coils or permanent magnets on the movers/translators, the proposed actuator is much suitable for applications of reciprocating oscillation. The simulated and experimental results in this paper will demonstrate that the TLSRA can be applied to linear compressors.

The organization of this paper is described as follows. In the section II, the model of linear compressors and the requirement

on the actuator force will be presented. Next, the proposed linear switched reluctance actuator with the tubular topology will be described, the analytical expression of gap permeance will be proposed, and the designed and experimental results will be shown in the section III. In the section IV, then, the model and experimental set-up of the linear compressor propelled by the proposed TLSRA will be presented. Furthermore, the simulated and experimental results will testify the proposed TLSRA. Finally, the paper will be concluded in the section V.

II. Linear Compressors Propelled by Linear Actuator

In applications of linear compressors, a linear actuator couples generally with a spring mechanically in parallel and the spring should work under resonance to provide the maximum propelling force and the maximum operating efficiency, as shown in Fig. 1a, where the spring is connected mechanically to the piston in parallel. The model of the system is illustrated in Fig. 1b.

Referring to Fig 1b, the motion equation can be given as

$$m\ddot{X} = F_{la} - (c_f + c_g)\dot{X} - (k_s + k_g)X \tag{1}$$

Consequently, the thrust force provided by the linear actuator

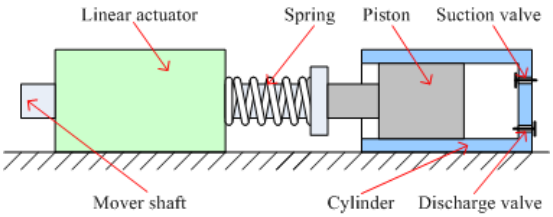

(a) Schematic structure of a linear compressor driven by a linear actuator

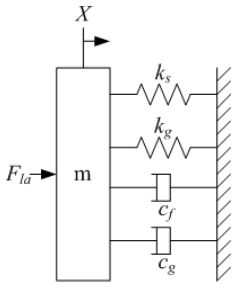

(b) Model of a linear compressor driven by a linear actuator

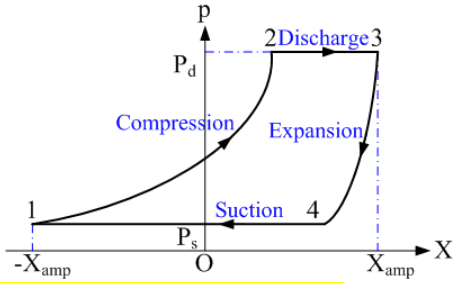

(c) Schematic diagram of a compression stroke

Fig. 1. Typical linear compressors driven by linear actuators

is expressed as

$$F_{la} = m\ddot{X} + (c_f + c_g)\dot{X} + (k_s + k_g)X \tag{2}$$

where F_{la} is the thrust force provided by the linear actuator, m the mass of all the motion parts, k_s the spring stiffness, c_f the friction damping coefficient, X the displacement of the piston, $\dot{X}$ the velocity of the piston, $\ddot{X}$ the acceleration of the piston, k_g the equivalent stiffness of the compressed gas, and c_g the equivalent viscous damping coefficient of the piston. k_g, c_f, c_g and the part of m in Fig. 1b arise from the linear compressor.

If the system runs under resonance, the resonant frequency is computed as [18]-[21]

$$f_r = \frac{\sqrt{\frac{k_s + k_g}{m}}}{2\pi} \tag{3}$$

The displacement of the piston should be the sinusoidal function with respect to the time if the spring operates under resonance, expressed as

$$X = X_m \sin(2\pi f_r t) \tag{4}$$

where X_m is the amplitude of the sinusoidal displacement , and t is the time.

Applying (4) to (2), the thrust force of the linear actuator is computed as

$$F_{la} = 2\pi f_r X_m (c_f + c_g) \cos(2\pi f_r t) \tag{5}$$

In order that the linear actuator outputs the thrust shown in (5), the coil current can be given as

$$i_c = f(F_{la}) \tag{6}$$

where the function (f) depends on the current-force characteristics of the linear actuator.

It can be observed from (5) that the thrust force provided by the linear actuator is required to be the cosine function of the time if the displacement is sinusoidal and the mechanical spring works under resonance. Furthermore, the frequency of the coil current should be equal to the resonant frequency as the frequency of the actuator force depends on the one of the coil current. In addition, it can be seen from (4) and (5) that the actuator force is equal to the force amplitude at the balance position of the piston (X=0) and thus the actuator force at the balance position must meet the requirement of the force amplitude in the electromagnetic design of the linear actuator. The schematic diagram is shown in Fig. 1c, where P_d is the discharge pressure, P_s the suction pressure, and p the pressure.

III. Proposed Tubular Linear Switched Reluctance Actuator

A. Structure of Proposed TLSRA

Conventional linear switched reluctance actuators (LSRAs) have the longitudinal magnetic structures [9]-[14]. In [15], the authors present the single-phase linear tubular switched reluctance motor and their study shows that the tubular linear

switched reluctance motor has the higher electromagnetic thrust force, the higher average thrust force per unit volume and the higher average thrust force per unit mass than conventional linear switched reluctance motors.

The TLSRA proposed in this paper possesses not only the longitudinal magnetic structure but also the transverse magnetic structure. For the proposed TLSRA, the transverse magnetic paths mainly exist in the stator cores and the mover cores and consist of four parts (ϕ_1-ϕ_4) as shown in Fig. 2a. The longitudinal magnetic paths exist mainly in the air gap if the stator poles are unaligned with the mover poles, as shown in Fig. 2b. It can be seen that there are two independent magnetic circuits. One of which consists of the stator core SA, the mover core MA, the stator winding WA and the air gap, and the other consists of the stator core SB, the mover core MB, the stator winding WB and the air gap, as shown in Fig. 2b. Thus, there are two stator windings and two stator cores, each stator core has four poles, and there is a coil on a pole. A stator winding consists of four coils connected in series or parallel. The converter circuit connected to two stator windings is shown in Fig. 2c, where I_{Ac} is the current path if the winding WA is charged and I_{Ad} is the current path if the winding WA discharges.

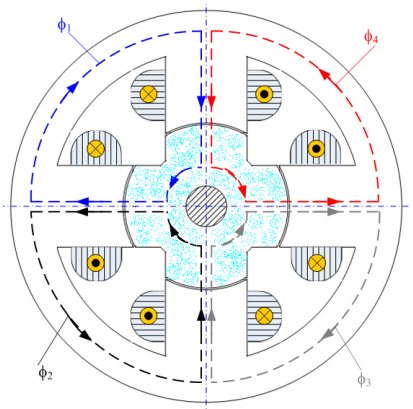

(a) Schematic diagram of transverse magnetic paths

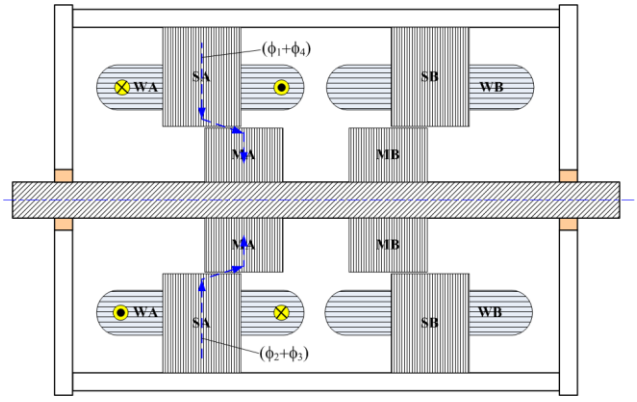

(b) Schematic diagram of longitudinal magnetic paths

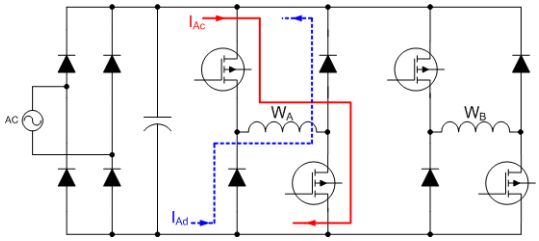

(c) Schematic diagram of converter circuit

Fig. 2. Proposed tubular linear switched reluctance actuators

Two stator windings are excited alternately in order that the mover moves to and fro. Changing the frequency of two winding currents, the resonant frequency can be traced. Regulating the magnitude of the exciting current, the travelled range of the mover can be changed [16]. In this study, the linear compressor requires the short travel range and consequently two phase windings are selected. For the applications of long travel range, multi-phase windings may be selected. Taking into account that the 4-pole structure has the more symmetrical distribution of radial force than the 2-pole structure, the 4-pole structure is used in this study.

Compared with linear PM actuators [1]-[8][18]-[21], it can be seen that the proposed TLSRA possesses the simple and robust configuration. Furthermore, there are no any both coils and magnets on the mover. Therefore, it has the lower cost and should be more suitable for applications of reciprocating motion. In comparison with conventional LSRAs [9]-[14], in addition, the proposed TLSRA has higher thrust force density and shorter magnetic flux paths. Clearly, for the same force output and the same dimensions, it can be predicted that the loss of the proposed TLSRA should be less than that of conventional LSRAs and the efficiency of the proposed TLSRA should be more than that of conventional LSRAs, due to the higher force density [15].

B. Key Design Equations

The magnetic gap resistance changes only with the mover displacement and has the great effect on the thrust force. Thus, the gap resistance is the crucial parameter in the

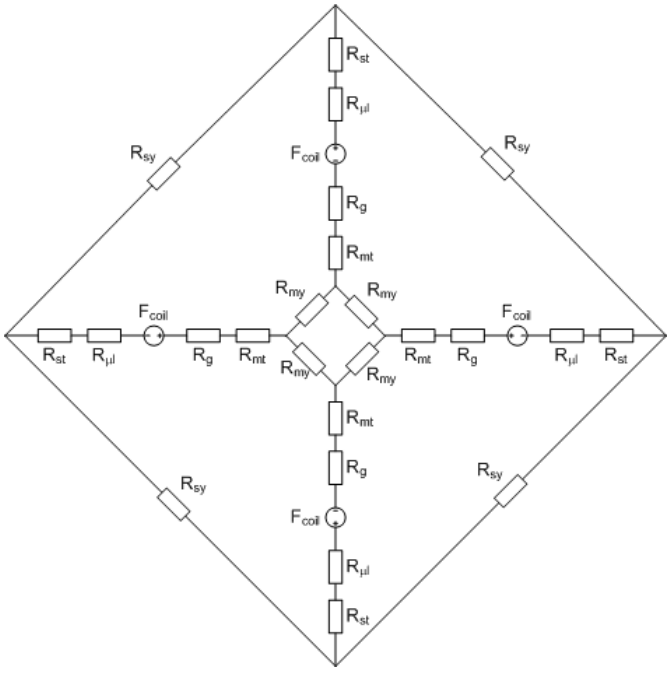

(a) Equivalent magnetic circuit

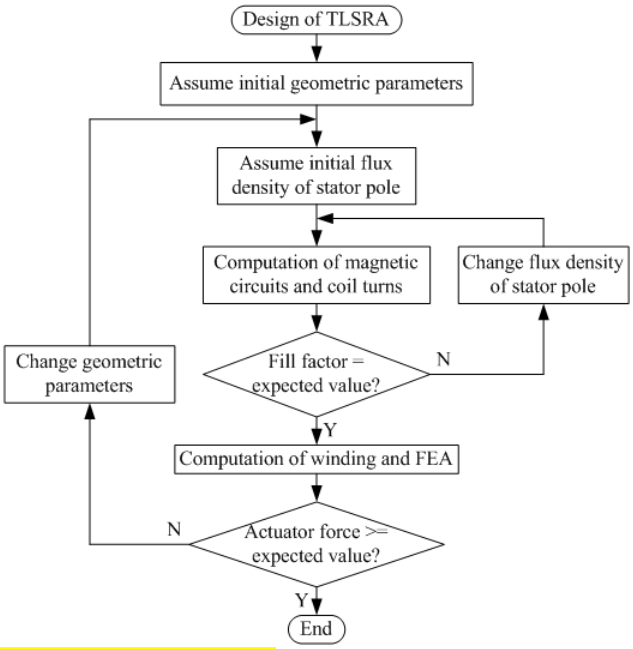

(b) Flowchart of TLSRA design

Fig. 3. Design schematic of TLSRA

electromagnetic design of the TLSRA. In general, the gap permeance at the special positions can be calculated analytically, such as the maximum gap permeance and the minimum gap permeance [10]. Consequently, it is difficult to compute the full force characteristics and the average force has to be computed rough to evaluate the force output in the conventional electromagnetic design. An analytical model of the gap permeance is presented in [17]. However, it results in the large error in the force computation.

Assuming that the displacement of the mover is zero if the stator pole is aligned with the mover pole in the longitudinal direction, the analytical expression of the magnetic gap reluctance is proposed as

$$R_g(x) = \frac{2}{a+b} \tag{7}$$

$$a = P_{gmax} + P_{gmin} \tag{8}$$

$$b = \frac{c}{1.05}\left(P_{gmax} - P_{gmin}\right) \tag{9}$$

$$c = \cos\left[\frac{\pi}{x_d}(x + x_0)\right] + 0.05\cos\left[\frac{3\pi}{x_d}(x + x_0)\right] \tag{10}$$

where x represents the displacement of the mover, P_{gmax} the maximum gap permeance, P_{gmin} the minimum gap permeance, x_d the distance between the position with the maximum gap permeance and the position with the minimum gap permeance, a, b, c and x_0 the intermediate variables, x_0=(x_d-w_{mp})/2, and w_{mp} the width of the mover pole.

The equivalent magnetic circuit and the design flowchart are illustrated in Fig. 3, respectively. Referring to Fig. 3a, the flux excited by the coil current can be expressed as

$$\phi = \frac{2(2-k_{\mu l})A_{st}N_c i}{d} \tag{11}$$

$$d = 2l_{st}/\mu_{st} + 2l_{mt}A_{st}/\mu_{mt}A_{mt} + l_{sy}A_{st}/2\mu_{sy}A_{sy} + l_{my}A_{st}/2\mu_{my}A_{my} + 2A_{st}R_g(x) \tag{12}$$

where $k_{\mu l}$ represents the magnetic leakage factor, A_{st} the equivalent area of the stator tooth path, N_c the number of the coil turns, i the coil current, l_{st} the equivalent length of the stator tooth path, μ_{st} the magnetic permeability of the stator tooth path, l_{mt} the equivalent length of the mover tooth path, μ_{mt} the magnetic permeability of the mover tooth path, A_{mt} the equivalent area of the mover tooth path, l_{sy} the equivalent length of the stator yoke path, μ_{sy} the magnetic permeability of the stator yoke path, A_{sy} the equivalent area of the stator yoke path, l_{my} the equivalent length of the mover yoke path, μ_{my} the magnetic permeability of the mover yoke path, and A_{my} the equivalent area of the mover yoke path.

The co-energy of the actuator is computed as

$$W'(i,x) = \int_0^i (N_{st}N_c\phi)di \tag{13}$$

where N_{st} represents the number of the stator teeth.

Thus, the thrust force of the actuator can be expressed as

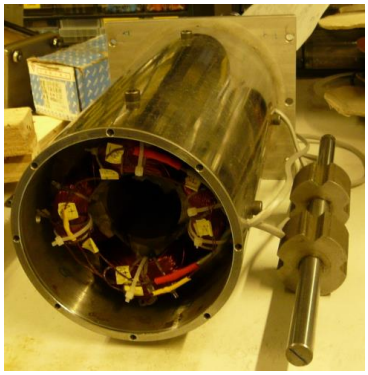

Fig. 4. Prototype of developed TLSRA

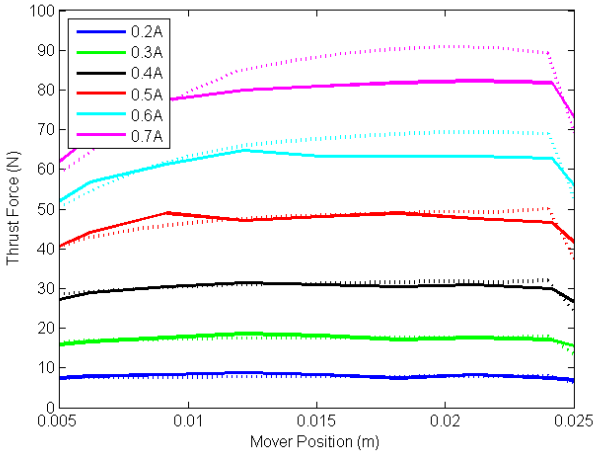

(a) Computed and measured thrust force characteristics (solid: experiment; dotted: FEA)

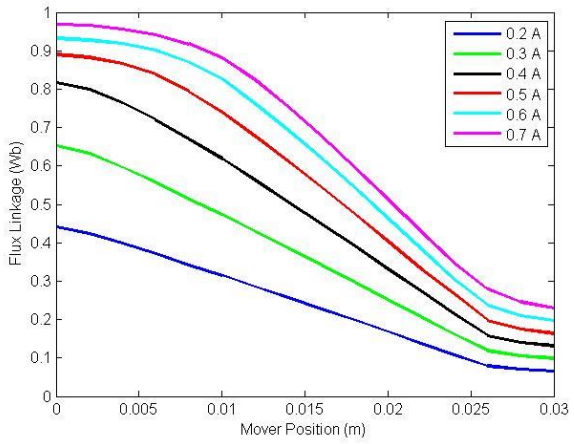

(b) Flux linkage characteristics computed by FEA

Fig. 5. Computed and measured characteristics of developed TLSRA prototype

$$f_{la}(i,x) = \frac{\partial W_f(i,x)}{\partial x}\Big|_{i=constant} \quad (14)$$

where f_{la}=0 if x=0.

C. Experimental Verification

The main parameters of the developed TLSRA prototype are described in Table I. The photo of the developed TLSRA prototype TLSRA is shown in Fig. 4.

The computed and measured characteristics of the developed TLSRA prototype are illustrated in Fig. 5. Referring to Fig.5a, the motion range of the mover can be selected from the position of 0.005 m to the one of 0.025 m in order to have the approximately constant force for a specified current.

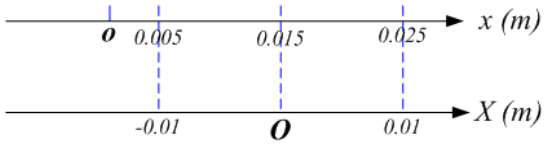

(a) *o*: aligned position of mover and *O*: balance position of piston

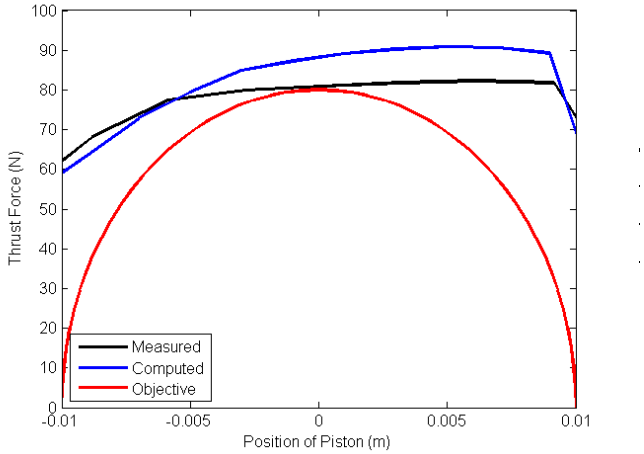

(b) Comparison between design objective, design computation and experiment at rated current

Fig. 6. Schematic diagram to select travelled range of piston

Furthermore, it can be seen that the force curves computed by using FEA (the dotted curves) are considerably consistent with the measured ones (the solid curves) in the selected motion range. Thus, the balance position of the piston (X=0, seeing (4)) is the one, at which the mover displacement is equal to 0.015 m and the thrust force amplitude is more than 80 N. Hence the mover is able to move by ±0.01 m, as shown in Fig. 6a. Fig. 6b shows the force distribution at the rated current and the design objective of the thrust force, which is the quasi-cosine function of the piston position and calculated from (4)-(5). It is obvious that the design meets the force requirement. It can be seen from Fig. 6b that the designed and measured values of the thrust force are more than the required objective of the thrust force. Consequently, the real thrust force can meet the required objective of the thrust force via the current control. Therefore, the results shown in Figs. 5-6 verify that the developed TLSRA prototype is effective and feasible, and matches the design requirement.

IV. Simulation and Experiment of Linear Compressor Propelled by Developed TLSRA

A. Dynamic Model

The proposed linear compressor system includes the TLSRA, the resonant spring, the piston and the cylinder. The control scheme of the linear compressor is illustrated in Fig. 7. The temperature controller is used to generate the required force amplitude based on the temperature reference and the actual temperature for keeping the actual temperature to trace the temperature reference. The temperature reference indicates the temperature instruction entered by a person and the actual temperature indicates the one measured by the device, such an air-conditioner. In this study, the temperature step is neglected and the force reference is given directly. The estimator of the input power is used to estimate the DC input power based on

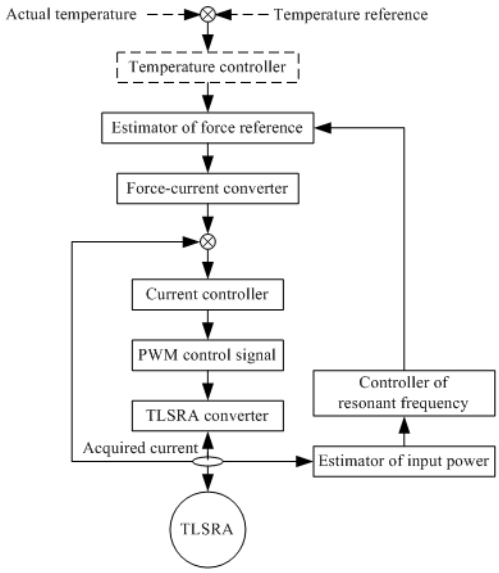

Fig. 7. Control scheme of linear compressor system

the acquired DC current. The controller of resonant frequency is used to find the resonant frequency of the spring based on the estimation of the input power. From the required force amplitude and the resonant frequency, the estimator of the force reference is used to generate the instantaneous force reference. The estimator of the force-current converter is used to compute the current reference from the force reference. The current controller is used to generate the PWM control signals for regulating the actual current via the TLSRA converter to trace the current reference. For the simulation, the required force amplitude will be given.

Except for (1) and (3), thus, the remaining equations of the dynamic system model are given as

$$F_{ref} = F_m \cos(2\pi f_r t) \tag{15}$$

$$i_{ref} = c_0 + c_1(F_{ref} - F_0) + c_2(F_{ref} - F_0)^2 + c_3(F_{ref} - F_0)^3 + c_4(F_{ref} - F_0)^4 \tag{16}$$

$$\frac{d\varphi}{dt} = v_w - r_w i_w \tag{17}$$

$$\varphi = f_\varphi(i_w, x) \tag{18}$$

$$F_{la} = f_F(i_w, x) \tag{19}$$

where F_{ref} is the force reference, F_m is the amplitude of the force reference, t is the time, i_{ref} is the winding current reference, c_0, c_1, c_2, c_3, c_4 and F_0 are the constants that are computed by using the least square algorithm, φ is the winding flux linkage that is computed by using FEA, v_w is the voltage across the winding, r_w is the winding resistance, i_w is the winding current, and x is the position of the actuator mover.

B. Simulated Results

Based on the proposed control scheme and the dynamic model, the linear compressor propelled by the proposed TLSRA can be simulated and studied. The simulated results are illustrated in Fig. 8, where F_{ref} represents the force reference for generating the current reference, I_{ref} the current reference for controlling the actual winding current, I_w the actual winding current, F_{la} the actual thrust force produced by the TLSRA, and X the displacement of the piston. In the simulation, it is assumed that the spring operates under resonance. Thus, the given force reference is computed from (15), as shown in the first diagram of Fig. 8a. Next, the current reference is computed from (16), as shown in the second diagram of Fig.8a. Then, the current controller is used to compute the PWM control output

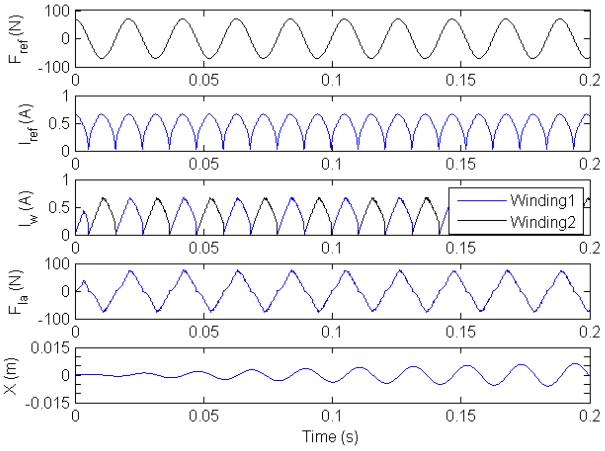

(a) During start

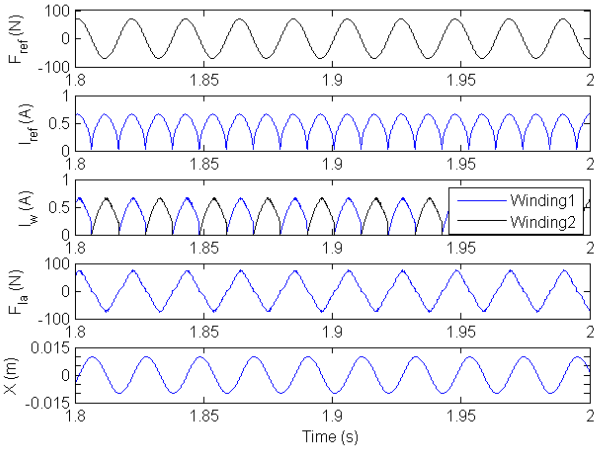

(b) During steady-state

Fig. 8. Simulated waveforms of force reference, current reference, real winding current, thrust force produced by TLSRA, and piston displacement

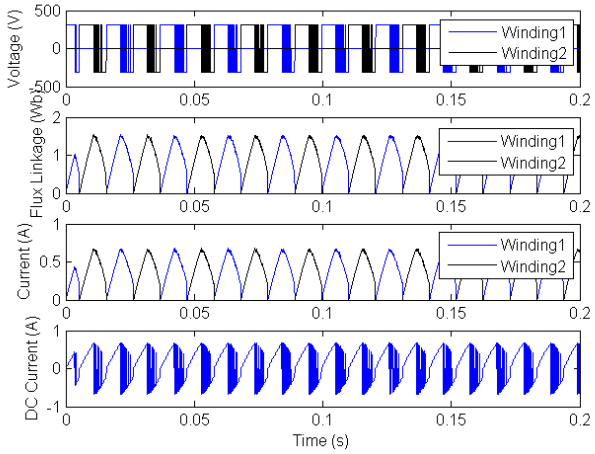

(a) During start

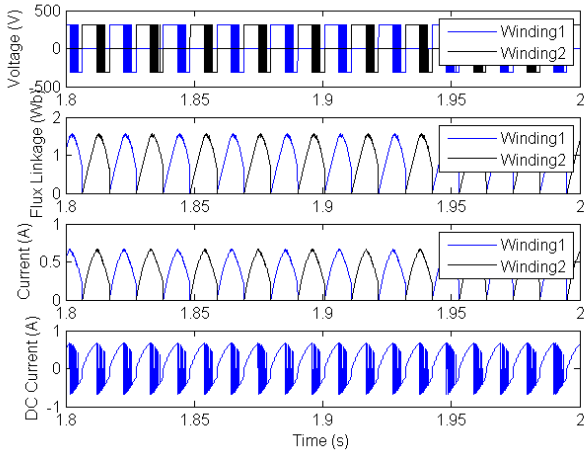

(b) During steady-state

Fig. 9. Simulated waveforms of voltage, flux linkage, real winding current, and DC link current

to the converter. After that, the TLSRA is simulated based on (1), (17)-(19) and the winding current, the TLSRA force and the displacement are simulated, as shown in the diagrams from the third to fifth ones of Fig. 8a. Fig. 8a illustrates the operation during the start, when the amplitude of the mover motion is increasing from 0 to large. Fig. 8b depicts the operation during the steady state, when the amplitude of the mover motion is the constant. The required force reference is the cosine function to the time as shown in (5) and thus the required current reference is the quasi-cosine function to the time due to the nonlinear relationship between the force and the current as shown in (16). Thereby, the PWM control is required to regulate the current via the converter for implementing the quasi-cosine current distribution to the time. Referring Fig. 8a, during the start, the amplitude of the mover motion changes from 0 to large and hence the operation is under dynamic state. Consequently, the actual force waveforms and the actual current waveforms are non-cosine shapes although the force reference is the cosine waveform and the current reference is the quasi-cosine waveform. In Fig. 8b, the amplitude of the mover motion does not change and the operation is under steady state. It can be seen from Fig. 8 that (a) the force reference changes in the form of cosine, (b) the current reference varies in the form of quasi-cosine since there is the nonlinear relationship between the force reference and the current reference, (c) both the actual current and the actual thrust force change in the form of quasi-cosine, and (d) the displacement of the piston varies in the form of sine and the amplitude of the piston increases from 0 to 0.01 m.

Fig. 9 depicts the simulated waveforms of the voltage across the windings, the flux linkage, the winding current, and the DC link current. It can be seen from Fig. 9 that (a) the voltage across two windings is controlled by the PWM control signal of the current controller such that the winding current is able to trace the current reference, and (b) there are the positive and negative DC link currents, which indicate that the electric energy arising from the TLSRA generation can be absorbed by the DC link and the system efficiency is improved. Furthermore, the displacement of the piston changes with the force reference. Consequently, the discharge pressure of the linear compressor can be regulated.

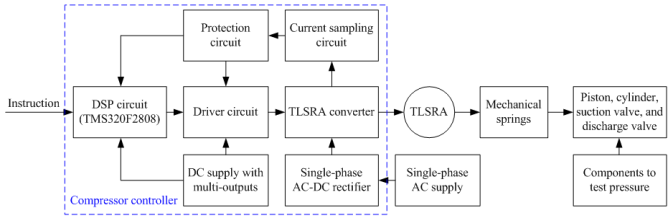

(a) Schematic structure of experimental set-up

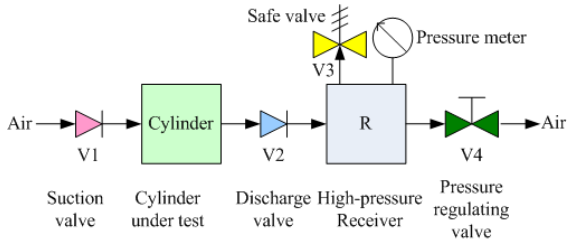

(b) Schematic diagram to test discharge pressure

Fig. 10. Schematic diagrams of experimental set-up for linear compressor propelled by TLSRA

C. Experiment

The set-up of the linear compressor propelled by the proposed TLSRA is constructed, as shown in Fig 10a. The schematic structure of the linear compressor system includes the compressor controller, the TLSRA, the mechanical springs, the piston, the cylinder, the suction and discharge valves. The compressor controller consists of the DSP circuit, DC supply circuit, driver circuit, sampling-current circuit, AC-DC rectifier circuit, and TLSRA converter circuit. The DSP circuit is used to receive the acquired current and the input instruction, to execute the computation, and to generate PWM control signals. The DC supply circuit is used to convert AC power to multi-output DC sources to supply the DSP circuit, driver circuit, and sampling-current circuit. The driver circuit is used to amplify the PWM control signals for driving MOSFETs in the TLSRA converter. The sampling-current circuit is used to acquire the actual winding currents. The AC-DC rectifier circuit is used to convert AC voltage to DC voltage. The TLSRA converter circuit is used to energize the windings in the TLSRA, to control and regulate the electric power input to the TLSRA. Fig. 10b illustrates schematic diagram for examining the discharge pressure of the set-up of the linear compressor. The air enters the cylinder via the suction valve (V1), in which the piston is propelled by the developed TLSRA via the springs. Via the discharge valve (V2), the pressed air enters the

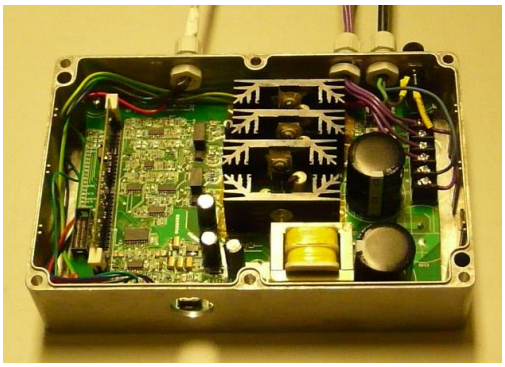

(a) Prototype of developed linear compressor controller

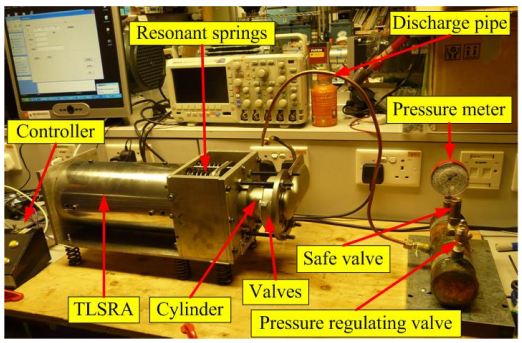

(b) Test rig of linear compressor propelled by proposed TLSRA

Fig. 11. Photos of prototypes

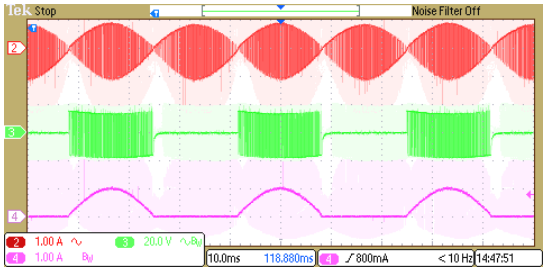

(a) Frequency reference = 30 Hz

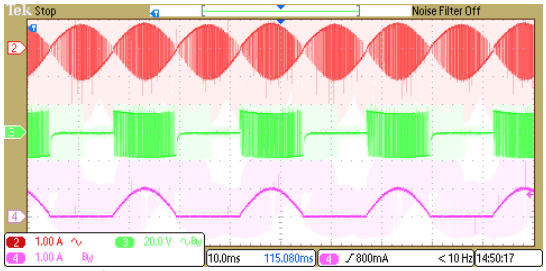

(b) Frequency reference = 40 Hz

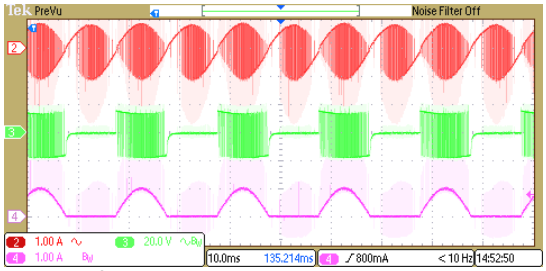

(c) Frequency reference = 50 Hz

Fig. 12. Measured waveforms at various frequencies with the current amplitude of 1.0 A (Trace 2: DC link current, 1 A/div; Trace 3: voltage across winding, 400 V/div; Trace 4: current in winding, 1 A/div)

high-pressure receiver, on which the safe valve (V3) is used to decompress for safe protection, the pressure meter is used to display the pressure in the receiver, and the valve (V4) is used to regulate the pressure in the receiver. The pressure value displayed on the pressure meter is the discharge pressure of the prototype of the developed linear compressor system.

The prototype of the compressor controller is shown in Fig. 11a and all the aforementioned circuits in the controller are integrated. The test rig of the linear compressor is depicted in Fig. 11b. It can be observed that the TLSRA, the springs, the cylinder, the piston and the valves are integrated.

Fig. 12 illustrates the measured current waveforms at various force references and frequencies. It can be seen from Fig. 12 that the developed compressor controller can output the various winding current waveforms depending on the current reference and frequency reference, and meet the requirement of the linear compressor, as the current and the frequency should be regulated at real-time to match the required force and resonant frequency.

The maximum displacement of the mover is measured by using the following approach. Firstly two boundary positions of the mover motion are marked during the prototype operation and then the distance between these two boundary positions is measured by the vernier caliper. The measured maximum displacement of the mover is 19.8 mm. It indicates that the measured amplitude of the mover is 9.9 mm, which is approximately equal to the simulated amplitude (10 mm). Consequently, it verifies the simulated result indirectly.

The measured discharge pressure of the linear compressor is over 8 bar if the refrigerant is selected as air. Therefore, the experiment has demonstrated that the proposed TLSRA can be used to propel the linear compressor and that the linear compressor driven by the proposed TLSRA is feasible.

V. Conclusion

The linear switched reluctance actuator with the tubular topology has been proposed for application to linear compressors. The actuator topology with hybrid magnetic structure and the main design equations have been presented. The prototype of the proposed TLSRA has been designed and fabricated. The computed and measured thrust force characteristics of the TLSRA prototype have verified the design and development of the TLSRA. Different from design of other types of machines, the force output of the TLSRA applied to linear compressors should be the quasi-cosine distribution to the mover displacement. Hence, the designed force values must be more than the required objective, which is distributed in the form of quasi-cosine.

The dynamic model of the linear compressor driven by the TLSRA has been proposed. The simulated results have demonstrated that the travelled range of the piston changes with the force reference and that the travelled range can reach to the design value. The test rig consisting of the TLSRA, the compressor controller, the resonant springs, the cylinder with the piston and the valves, and the pressure measurement components has been constructed. The simulated and experimantal results have verified that the proposed TLSRA can be applied to linear compressors and that the developed linear compressor propelled by the proposed TLSRA is feasible. In the experiment, the performance of the linear compressor system degraded due to the friction between the mechanical springs and the frame as well as the leakage of the mechanical connection between the piston, cylinder and valves. Otherwise, the developed linear compressor system should demonstrate the better performance. Due to simple and robust configuration, therefore, the proposed TLSRA is a promising candidate for applications to linear compressors and other reciprocating motion.

Appendix

The calculation of the maximum gap permeance and the minimum gap permeance is given as follows [10].

$$P_{gmax1} = \mu_0 w_{st} \frac{w_{sp}}{l_g} \quad \text{(A1)}$$

$$P_{gmax2} = 0.264 \mu_0 w_{st} \quad \text{(A2)}$$

$$P_{gmax3} = 0.318 \mu_0 w_{st} \ln\left(1 + 2\frac{h_{st}/12}{l_g}\right) \quad \text{(A3)}$$

$$P_{gmax4} = 0.268 \mu_0 w_{sp} \quad \text{(A4)}$$

$$P_{gmax5} = 0.318 \mu_0 w_{sp} \ln\left(1 + \frac{h_{st}}{6 l_g}\right) \quad \text{(A5)}$$

$$P_{gmax6} = 0.076\mu_0 l_g \quad \text{(A6)}$$

$$P_{gmax7} = 0.25\mu_0 \frac{h_{st}}{12} \quad \text{(A7)}$$

$$P_{gmax} = P_{gmax1} + 2\left(P_{gmax2} + P_{gmax3}\right) + 4\left(P_{gmax4} + P_{gmax5} + P_{gmax6} + P_{gmax7}\right) \quad \text{(A8)}$$

$$d_1 = x_d - \frac{w_{sp}+w_{mp}}{2} \quad \text{(A9)}$$

$$d_2 = d_1 - l_g \quad \text{(A10)}$$

$$P_{gmin1} = \mu_0 w_{st} \frac{d_2}{2d_1} \quad \text{(A11)}$$

$$P_{gmin2} = 0.134\mu_0 w_{st} \quad \text{(A12)}$$

$$P_{gmin3} = 0.134\mu_0 t_5 \quad \text{(A13)}$$

$$P_{gmin} = P_{gmin1} + P_{gmin2} + 2P_{gmin3} \quad \text{(A14)}$$

where μ_0 represents the vacuum permeability, w_{st} the width of the stator tooth, w_{sp} the width of the stator pole, l_g the length of the air gap, and h_{st} the height of the stator tooth.

ACKNOWLEDGMENT

REFERENCES

[1] Ross A. Howard, Yimin Xiao, and Steven D. Pekarek, "Modeling and Design of Air-Core Tubular Linear Electric Drives", *IEEE Transactions on Energy Conversion*, vol. 28, DOI 10.1109/TEC.2013.2275771, no. 4, pp. 793-804, Dec. 2013.

[2] Yuqiu Zhang, Qinfen Lu, Minghu Yu_, and Yunyue Ye, "A Novel Transverse-Flux Moving-Magnet Linear Oscillatory Actuator", *IEEE Transactions on Magnetics*, vol. 48, DOI 10.1109/TMAG.2011.2178077, no. 5, pp. 1856-1862, May 2012.

[3] Cristofaro Pompermaier, Kalluf Flavio Jorge Haddad, Alexandre Zambonetti, M. V. Ferreira da Luz, and Ion Boldea, "Small Linear PM Oscillatory Motor: Magnetic Circuit Modeling Corrected by Axisymmetric 2-D FEM and Experimental Characterization", *IEEE Transactions on Industrial Electronics*, vol. 59, DOI 10.1109/TIE.2011.2161650, no. 3, pp. 1389-1396, Mar. 2012.

[4] I. BOLDEA and SA. NASAR, "LINEAR ELECTRIC ACTUATORS AND GENERATORS", *IEEE Transactions on Energy Conversion*, vol. 14, no. 3, pp. 712-717, September 1999.

[5] J. Wang Z. Lin D. Howe, "Analysis of a short-stroke, single-phase, q uasi-Halbach magnetised tubular permanent magnet motor for linear compressor applications", *IET Electr. Power Appl.*, vol. 2, DOI 10.1049/iet-epa:20070281, no. 3, pp. 193–200, 2008.

[6] Qinfen Lu, Minghu Yu, Yunyue Ye, Youtong Fang, and Jianguo Zhu, "Thrust Force of Novel PM Transverse Flux Linear Oscillating Actuators with Moving Magnet", *IEEE Transactions on Magnetics*, vol. 47, DOI 10.1109/TMAG.2011.2157991, no. 10, pp. 4211-4214, 2011.

[7] S. A. Evans, I. R. Smith, and J. G. Kettleborough, "Permanent-Magnet Linear Actuator for Static and Reciprocating Short-Stroke Electromechanical Systems", *IEEE/ASME Transactions on Mechatronics*, vol. 6, DOI 10.1109/3516.914389, no. 1, pp. 36-42, MARCH 2001.

[8] Zhang Chunping, Guo Fangzhong, Zhang Xiaoqing, Liu Wei, "Design of miniature moving magnet linear actuator for thermoacoustic Stirling system", *2010 Asia-Pacific Power and Energy Engineering Conference* (APPEEC), DOI 10.1109/APPEEC.2010.5448858, pp. 1-4, 2010.

[9]

[10] R. Krishnan, *Switched Reluctance Motor Drives - Modeling, Simulation, Analysis, Design, and Applications*, CRC Press, 2001, pp. 141-167.

[11]

[12]

[13] Yiming Shen, Qinfen Lu, Huanwen Li, Jiongjiong Cai, Xiaoyan Huang, and Youtong Fang, "Analysis of a Novel Double-sided Yokeless Multi-tooth Linear Switched-flux PM Motor", *IEEE Transactions on Industrial Electronics*, DOI 10.1109/TIE.2017.2696492, accepted for publication in a future issue.

[14] Jordi Garcia-Amorós, Pere Andrada, Balduí Blanque and Marc Marin Genesca, "Influence of Design Parameters in the Optimization of Linear Switched Reluctance Motor under Thermal Constraints", *IEEE Transactions on Industrial Electronics*, DOI 10.1109/TIE.2017.2686361, accepted for publication in a future issue.

[15] Hao Chen, Rui Nie, and Wenju Yan, "A Novel Structure Single-phase Tubular Switched Reluctance Linear Motor", *IEEE Transactions on Magnetics*, DOI 10.1109/TMAG.2017.2700007, accepted for publication in a future issue.

[16]

[17] J. F. Gieras and Z. J. Piech, "Chapter 3.4.2 Reluctance Network Approach" in *Linear Synchronous Motors - Transportation and Automation Systems*, CRC Press, 2000.

[18] Joseph Latham, Michael L. McIntyre, and Mohammad Mohebbi, "Parameter Estimation and a Series of Nonlinear Observers for the System Dynamics of a Linear Vapor Compressor", *IEEE Transactions on Industrial Electronics*, vol. 63, DOI 10.1109/TIE.2016.2582728, no. 11, NOVEMBER 2016, pp. 6736-6744.

[19] Zhengyu Lin, Jiabin Wang, and David H, "A Learning Feed-Forward Current Controller for Linear Reciprocating Vapor Compressors", *IEEE Transactions on Industrial Electronics*, vol. 58, DOI 10.1109/TIE.2010.2089948, no. 8, AUGUST 2011, pp. 3383-3390.

[20] Jiabin Wang, David Howe, and Zhengyu Lin, "Design Optimization of Short-Stroke Single-Phase Tubular Permanent-Magnet Motor for Refrigeration Applications", *IEEE Transactions on Industrial Electronics*, vol. 57, DOI 10.1109/TIE.2009.2025710, no. 1, JANUARY 2010, pp. 327-334.

[21] Tae-Won Chun, Jung-Ryol Ahn, Hong-Hee Lee, Heung-Gun Kim, and Eui-Cheol Nho, "A Novel Strategy of Efficiency Control for a Linear Compressor System Driven by a PWM Inverter", *IEEE Transactions on Industrial Electronics*, vol. 55, DOI 10.1109/TIE.2007.909730, no. 1, JANUARY 2008, pp. 296-301.